ELSEVIER

Journal of Magnetism and Magnetic Materials 221 (2000) 327–337

Journal of magnetism and magnetic materials

www.elsevier.com/locate/jmmm

Temperature evolution of the internal magnetic hyperfine field of Metglas: amorphous and crystallized phases

V. Marquina[a,*], R. Gómez[a], M. Jiménez[a], R. Ridaura[a], M.L. Marquina[a], R. Escamilla[b], M. Miki[c]

[a]*Facultad de Ciencias, UNAM. Circuito Exterior, CU 04510 México D.F., Mexico*
[b]*Instituto de Investigaciones en Materiales, UNAM Circuito Exterior, CU 04510 México D.F., Mexico*
[c]*Centro de Investigación en Materiales Avanzados, A.C. Chihuahua, Chih., Mexico*

Received 28 March 2000; received in revised form 20 July 2000

Abstract

We present differential scanning calorimetry (DSC), X-ray diffractometry, in situ Mössbauer spectroscopy (MS), and transmission electron microscopy (TEM) studies in Metglas ribbons subjected to different heat treatments. The temperature evolution of the hyperfine field $H_{hf}(T)$ and the Curie temperature (T_c) of the amorphous phase are determined. The magnetic field originally present in the amorphous phase has a 'normal' behavior, in the sense that it can be described by the Weiss molecular field theory. The total angular momentum of the iron atoms turns out to be 5/2 and this implies Fe^{3+} in which the electronic spins are uncoupled. When the samples are maintained near T_c (≈ 673 K), three new magnetic phases are detected in the Mössbauer spectra, indicating an onset of a crystallization process well below the first crystallization temperature (T_{X1}), as determined by DSC (≈ 820 K). The magnetic behavior of these phases is also described by universal Brillouin curves with $J_1 = \frac{3}{2}, J_2 = \frac{5}{2}$ and $J_3 = \frac{5}{2}$. A pre-identification of the crystalline phases is made through the Mössbauer parameters of the three observed magnetic phases, and the final characterization by X-ray and electron diffraction. Two of the three phases were identified as α-FeSi and Fe_2B. The third phase could be the cubic phase of Fe_3Si or a solid solution of FeSi. The size of the nanocrystals formed in a sample heated at 673 K during different time intervals were determined by TEM. Even though the number of the nanocrystals increases with time, their average size remains the same.

PACS: 75.50.Kj; 61.43.Dq; 76.80. + y; 61.18.Fs

Keywords: Metallic glass; Amorphous ferromagnet; Mössbauer spectroscopy; X-ray

1. Introduction

The importance of ferromagnetic metallic glasses arises not only because of their possible applications, but also from the point of view of the basic physics involved [1,2] in their behavior. From this point of view, the fact that amorphous alloys showed ferromagnetic behavior changed the conception that long-range order was essential for this property [3]. On the other hand, the nanocrystallization of an amorphous ferromagnet, as a consequence of heat treatments, may produce substantial

* Corresponding author. Tel.: + 525-6224849; fax: + 525-6160326.
E-mail address: marquina@servidor.unam.mx (V. Marquina).

0304-8853/00/$ - see front matter
PII: S0304-8853(00)00496-0

softening in its magnetic properties, presumably by a randomization of magnetic anisotropy, and a decrease of their magnetostriction constant [4]. However, the exact nature of the changes involved in the nanocrystallization process is not fully understood [5].

This paper deals mainly with the thermal evolution of the magnetic properties of Metglas® 2605 SC amorphous ribbons (nominal composition: $Fe_{81}B_{13.5}Si_{3.5}C_2$). An advantage of this material is its high iron content, which allows the use of Mössbauer spectroscopy to study the variations of the internal hyperfine field due to different causes, as those produced by thermal or thermomechanical treatments. We also report the results of DSC, X-ray diffraction and TEM.

2. Experimental techniques

All the measurements were performed on small pieces of about 1 cm^2 cut from commercial Metglas. The calorimetric measurements were performed in a Dupont 2100 differential scanning calorimeter, using a heating rate of 15°C/min.

The Mössbauer spectra (MS) were recorded using a constant acceleration spectrometer with transmission geometry and a ^{57}Co in Rh source kept at room temperature. All the spectra were recorded in situ, placing the absorbers on the sample holder of a vacuum furnace, or of a closed cycle refrigeration system. The obtained spectra were fitted using a constrained least-squares program. The temperature evolution of the hyperfine field in the amorphous phase was studied from 13 K up to its Curie temperature ($T_c \approx 673$ K), whereas for the crystalline phases the interval was from the Curie temperature of each of the crystalline phases (T_c^*) to room temperature.

The X-ray diffractograms were recorded in a Siemens D-5000 operating at 30 kV and 35 mA. The Cu K_α line radiation monochromated with a graphite filter was used. Four diffractograms were recorded: one for the as-cast material and three more for samples that were annealed in an inert atmosphere at 753 K (80 K above T_c, as judged from the DSC curve) for 12, 18 and 48 h, and then slowly cooled to room temperature.

Transmission electron microscopy (TEM) micrographs and electron diffraction patterns were obtained with a Jeol Electron Microscope CM-200. A disk-shaped sample of the as-cast material, 3.0 mm in diameter, was thinned with an argon ion jet in a PIPS-691 system and then placed in the lateral entrance goniometer of the microscope, operated at 200 kV (0.27 nm resolution). The sample was heated at 100 K/min up to $T_c = 673$ K and maintained at that temperature for different time periods.

3. Results

The DSC curve is shown in Fig. 1. Apart from two huge exothermic peaks associated with the crystallization processes that occur at $T_{X1} \approx 820$ K and $T_{X2} \approx 826$ K, there is a broad feature between 673 and 725 K that can be associated, as will be clear later, with the ferromagnetic to paramagnetic phase transformation of the system. Guided by the DSC results, a systematic study of the Mössbauer spectra at different temperatures was carried out. The as-cast room temperature MS exhibited a six line magnetic structure (Fig. 2) with broad lines. To provide more information on the magnetic field evolution, a spectrum at 13 K was also recorded (Fig. 3). In Figs. 4–7 we show the *in situ* recorded spectra at different temperatures, ranging from 440 to 673 K. The time during which each spectrum was taken is indicated in the figure captions. The

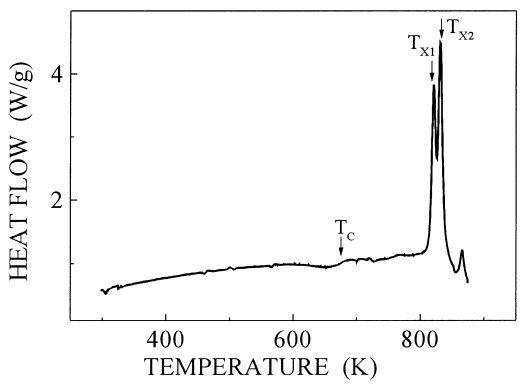

Fig. 1. Differential scanning calorimetry curve (15°C/min).

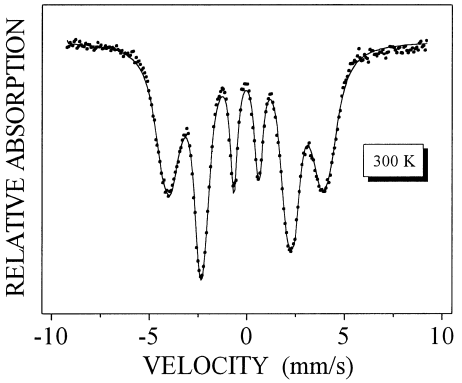

Fig. 2. Room temperature MS (12 h accumulation).

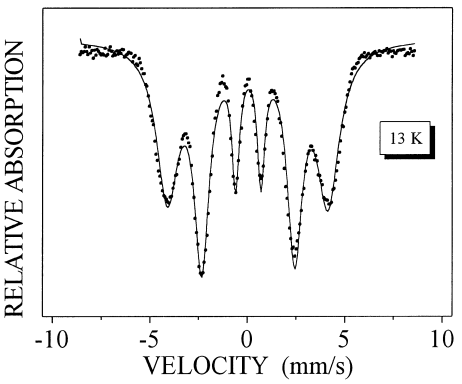

Fig. 3. MS at 13 K (12 h accumulation).

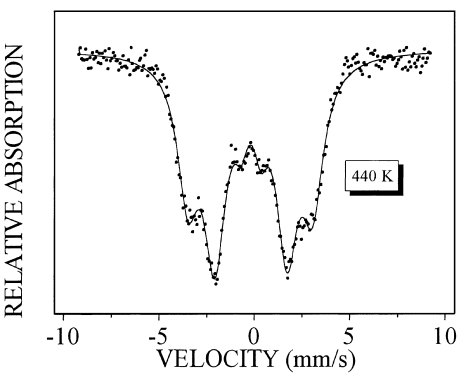

Fig. 4. MS at 440 K (12 h accumulation).

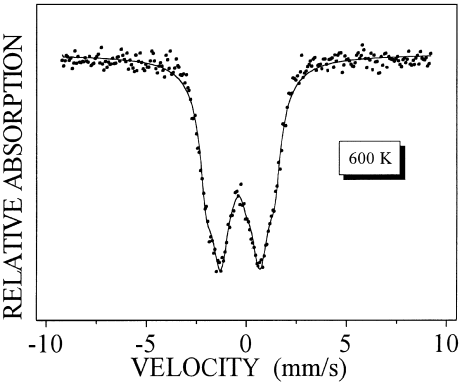

Fig. 5. MS at 600 K (12 h accumulation).

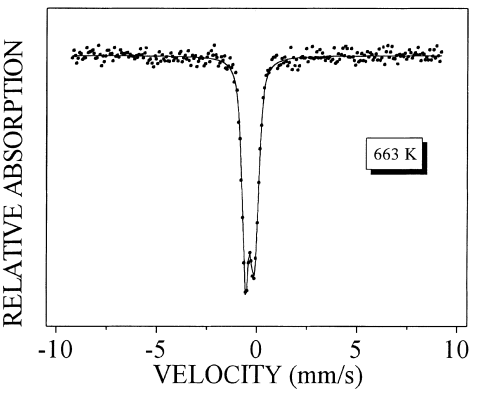

Fig. 6. MS at 663 K (2 h accumulation).

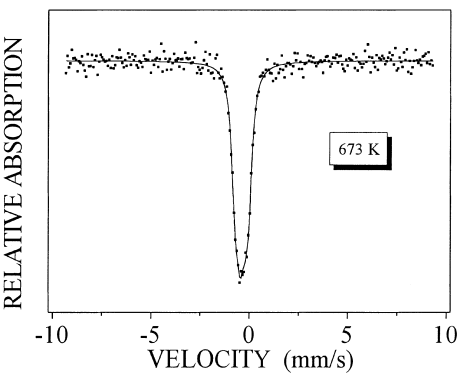

Fig. 7. MS at 673 K (1.5 h accumulation).

continuous line in each spectrum is the result of the fitting process with a single magnetic sextet and no restriction to the linewidths, so that the obtained values represent an average hyperfine field. Apart from the wideness of the spectral peaks, it is worth mentioning that, in all cases, the quadrupole splitting is essentially zero, as has been proven by Chien [6].

As the temperature is increased, there is a gradual reduction of the hyperfine field until a paramagnetic singlet appears. The changes in the magnetic field intensities observed in a temperature interval that ranges from 13 K to around 650 K are essentially reversible, indicating that the amorphous character of the material does not change in this temperature interval. Nevertheless, the relative intensities of the different hyperfine lines vary slightly. These slight changes must be associated with the release of mechanical strains produced during the fast cooling of the material. The reversibility is maintained even if the sample is kept for a short time (few minutes) at, or near, the Curie temperature. However, if the sample is heated at $T_c = 673$ K during 12 h, a new magnetic field begins to evolve, that superimposes on the paramagnetic one. Fig. 8 shows the spectrum of the sample heated to 673 K and maintained at this temperature for 12 h, after the spectrum of Fig. 7 was recorded. This indicates that the crystallization process has begun well below the crystallization temperatures (T_{X1} and T_{X2}). A new spectrum was recorded at the same temperature (673 K) and the result is shown in Fig. 9. Surprisingly no trace of the residual amorphous fraction (no paramagnetic peak) is seen in this spectrum. Fig. 10 shows the temperature variation of the measured average magnetic field of the amorphous phase.

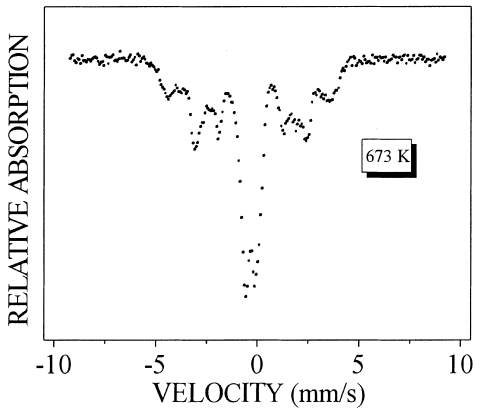

Fig. 8. MS at 673 K (1.5 h + 12 h accumulation).

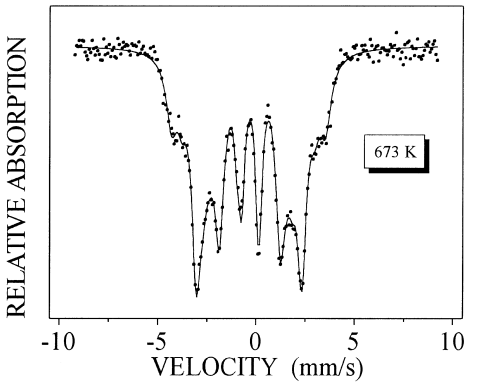

Fig. 9. New MS at 673 K restarting the accumulation after the MS of Fig. 8 was recorded (9 h accumulation).

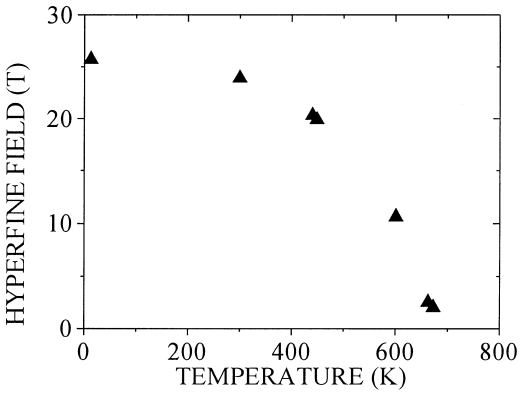

Fig. 10. Temperature variation of the amorphous phase hyperfine magnetic field.

To assure a complete crystallization a new sample was heated for 12 h at 900 K and then slowly cooled to room temperature. In the MS of that sample recorded at 300 K, three unexpected hyperfine subspectra were obtained (Fig. 11), indicating the presence of new magnetic phases. In this figure we show the three subspectra separately by dotted lines.

In order to identify the magnetic phases (and maybe the crystalline phases) systematic studies of

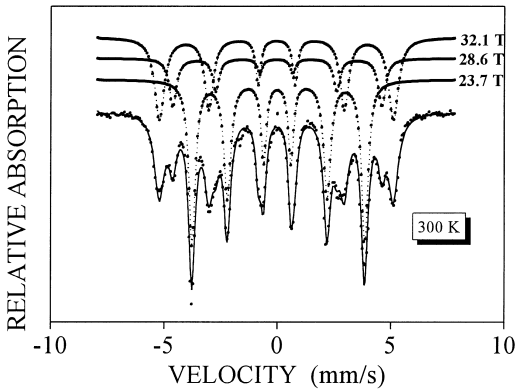

Fig. 11. Room temperature MS of the crystallized sample.

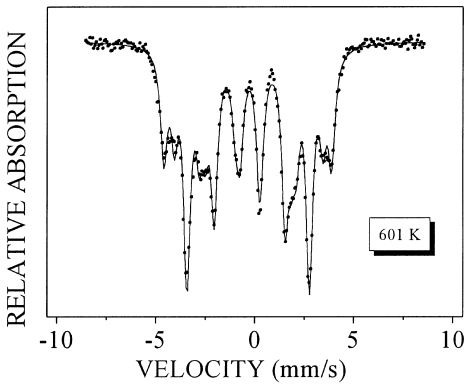

Fig. 12. MS of the crystallized sample at 601 K.

the temperature evolution of the new hyperfine fields were performed, from room temperature up to a temperature ($T_c^* = 933$ K) such that the resulting spectrum showed a single paramagnetic line; that is, until all the three magnetic phases had become paramagnetic. Figs. 12–15 show the typical spectra obtained in these cases. The continuous line in each spectrum is the result of a fitting process in which the linewidths were fixed to a value close to the natural linewidth, so that the magnitudes of the hyperfine fields are not average values, as in the amorphous case. Their temperature variations are shown in Fig. 16. Once again, all the quadrupole splittings are essentially zero.

To obtain information about the crystalline phases and crystal formation kinetics, an X-ray diffraction study was also made in four samples:

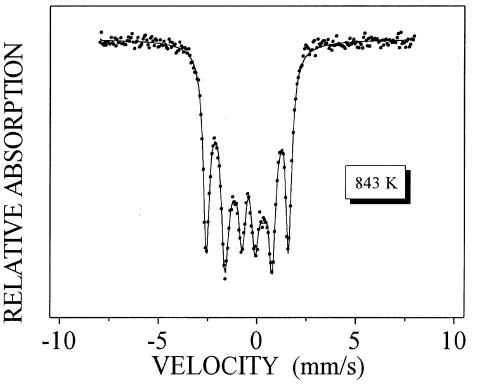

Fig. 13. MS of the crystallized sample at 843 K.

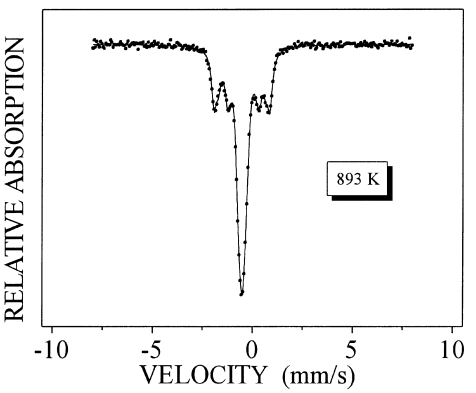

Fig. 14. MS of the crystallized sample at 893 K.

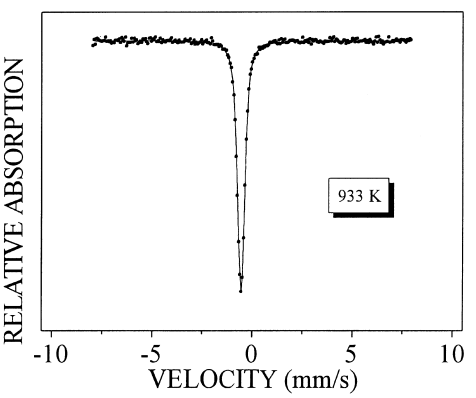

Fig. 15. MS of the crystallized sample at 933 K.

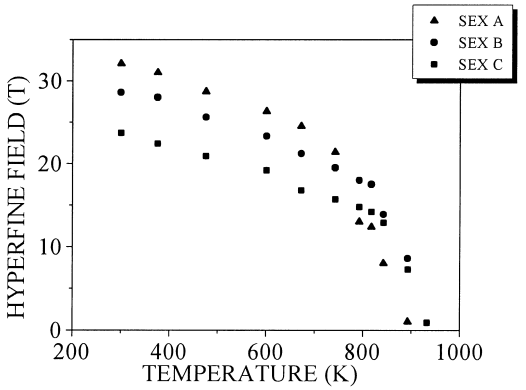

Fig. 16. Temperature variation of the three hyperfine fields.

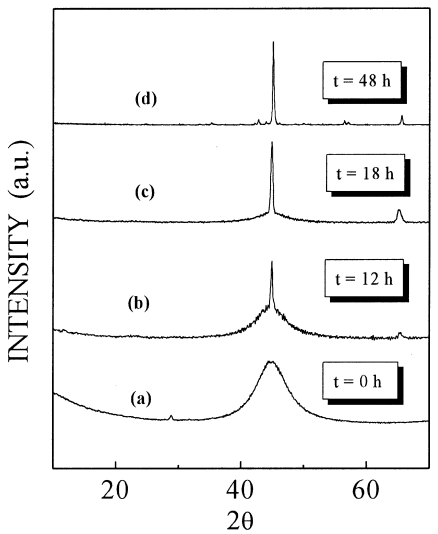

Fig. 17. X-ray diffractograms of Metglas: (a) *as-cast,* and heat treated at 753 K, during (b) 12, (c) 18 and (d) 48 h.

one as-cast and the other three, heat treated at 753 K (80 K above the T_c) for 12, 18 and 48 h in inert (N_2) atmosphere. The results are shown in Fig. 17, in which the evolution from the amorphous to the crystalline state can be seen.

TEM micrographs (MG) and electron diffraction patterns (EDP) were first recorded at room temperature. Then the sample was heated in situ at 100 K/min up to 673 K. New MG-EDP were obtained after 3–5, 12–13 and 60–61 min (Fig. 18). Two important things are to be noted in these results: firstly, the crystallization of a large fraction of the material after 3 min (Figs. 18c and d) and secondly, the size (20 nm in average) of the nanocrystals does not increase with the time of the heat treatment (Figs. 18d, f and g).

4. Discussion

Notwithstanding the random fluctuations of the exchange interaction present in an amorphous material, the existence of a magnetic field at room temperature is a clear manifestation that these fluctuations do not average to zero. The description of this effect can be made via a homogeneous [7] or an inhomogeneous [8] molecular field approximation. In any case, the magnetization of the material is expected to follow the Weiss molecular field theory [9]. In order to study the behavior of this average effect, no restriction was put on the linewidths during the fitting process of the MS, in such a way that the magnetic field intensities so obtained represent an average value of the hyperfine field.

The evolution of the Mössbauer spectra with increasing temperature, shown in Figs. 4–6, is due to a decrease of the hyperfine field, until a paramagnetic peak is obtained at $T_c = 673$ K (Fig. 7), in good agreement with the first feature observed in the DSC curve. The average magnetic field intensity as a function of temperature $H_{hf}(T)$ is shown in Fig. 10. This curve was fitted assuming that the hyperfine field is given by Weiss molecular field theory; i.e.,

$$\frac{H_{hf}(T)}{H_{hf}(0)} = B_J(x), \tag{1}$$

where $B_J(x)$ is the Brillouin function and $H_{hf}(0)$ is the zero kelvin extrapolated hyperfine field

$$B_J(x) = \frac{2J+1}{2J}\coth\left[\left(\frac{2J+1}{2J}\right)x\right] - \frac{1}{2J}\coth\left[\left(\frac{1}{2J}\right)x\right]. \tag{2}$$

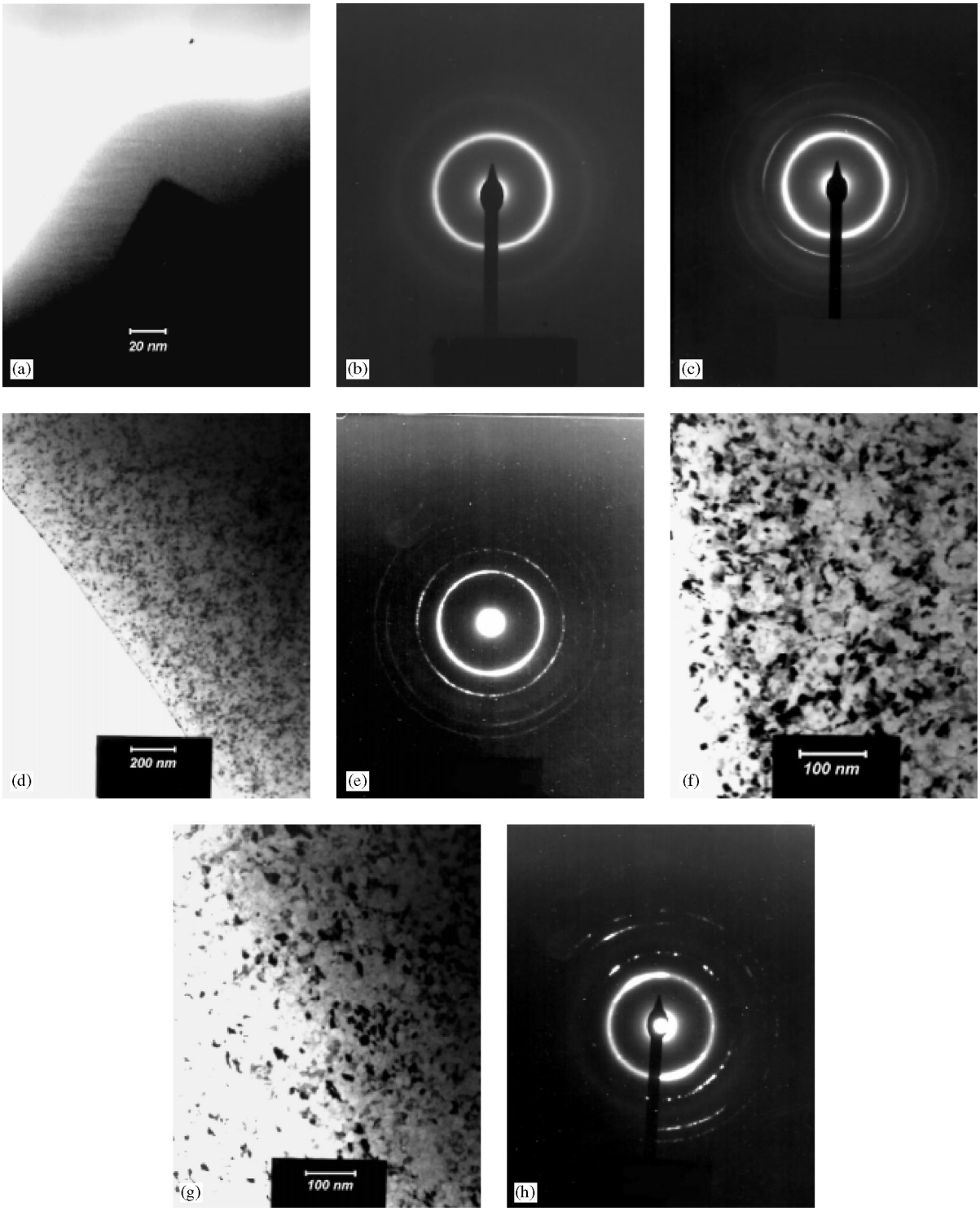

Fig. 18. In situ EDP and MG of a Metglas sample heated at 673 K; (a) As-cast; (b) As cast; (c) 3 min; (d) 5 min; (e) 12 min; (f) 13 min; (g) 60 min; and (h) 61 min.

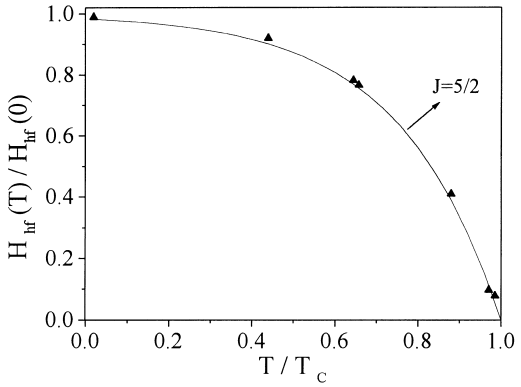

Fig. 19. Normalized hyperfine field as a function of normalized temperature.

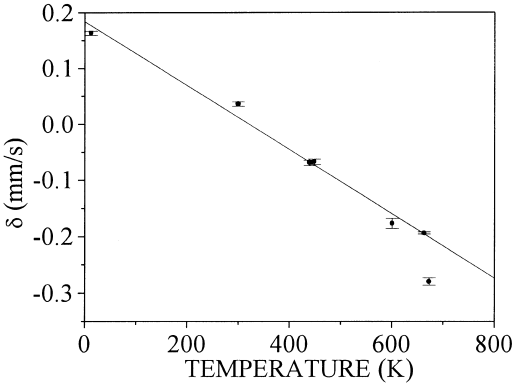

Fig. 20. Temperature variation of the isomer shift of the amorphous phase.

J is the total angular momentum of the magnetic atoms, and $x = g\mu_B H_{hf} J/k_B T$, where μ_B is the Bohr magneton, g the Landè factor and k_B is the Boltzmann constant.

Solving this equation [10], the theoretical curve that best fits the experimental data was obtained using $J = \frac{5}{2}$ and it is shown in Fig. 19. The $J = \frac{5}{2}$ value of the total angular momentum obtained in the fitting process implies a $3+$ ionic state of the iron atoms in which the electron spins are uncoupled. These uncoupled spins must be a characteristic of the amorphous state of the material. On the other hand, the small value of the magnitude of the magnetic field must be the manifestation of the large average separation of the magnetic atoms in the amorphous phase, compared with the same separations in the crystalline state. It could also indicate a smaller interchange coupling constant due to the lack of a translational symmetry. In this sense, it is interesting to note two experimental facts: in the first place, the temperature variation of the isomer shift, δ, (Fig. 20) follows the usual second-order Doppler behavior [11] except near T_c, where a discontinuous jump is observed [12,13]. In the second place, the experimental values of $H_{hf}(T)/H_{hf}(0)$ also deviate from the theoretical curve near T_c. One possible reason for these behaviors could be that a small fraction of the amorphous phase begins to crystallize, as it is revealed by the presence of a new (different) hyperfine field when the sample is maintained 12 h at 673 K (Fig. 8), well below the DSC crystallization temperature. Albeit the intrinsic sensitivity of Mössbauer spectroscopy, this crystallization is only noticeable as a magnetic sextet after sufficient time has elapsed (12 h at 673 K), so as to make the intergranular distances shorter than the exchange correlation length (around 40–50 nm [14]). That is to say, even if a nanocrystallization process begins, the size of the crystals is so small and their average separation is so large, that no magnetic coupling takes place between them and the rest of the amorphous phase. The magnitude of the new magnetic field is now characteristic of the crystalline state and no traces of the amorphous material can be seen in the MS. However, the X-ray and TEM results show that the material is far from being totally crystallized. This could be understood assuming that once the average separation between the nanocrystals is shorter than the correlation length, the local magnetic field magnetizes the surrounding amorphous material and the paramagnetic singlet disappears.

The MS of the sample annealed at 673 K during 12 h is more complex than the ones of the amorphous phase and apparently consists of two magnetic sextets. However, when the MS of this sample was recorded at room temperature (Fig. 12), an unexpected result was obtained. Now, the presence of at least three magnetic subspectra is evident and assuming the presence of three different magnetic phases, a good fit could be obtained for all the spectra recorded once the material crystallized.

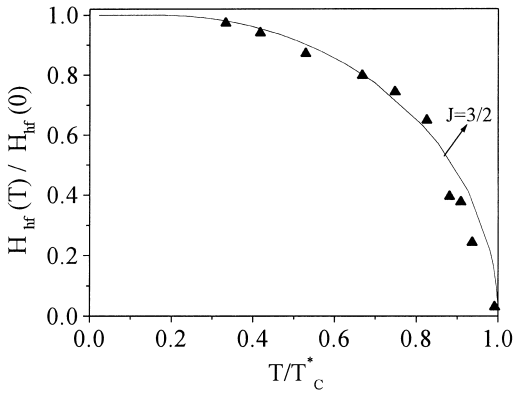

Fig. 21. Normalized hyperfine field as a function of normalized temperature of sextet A.

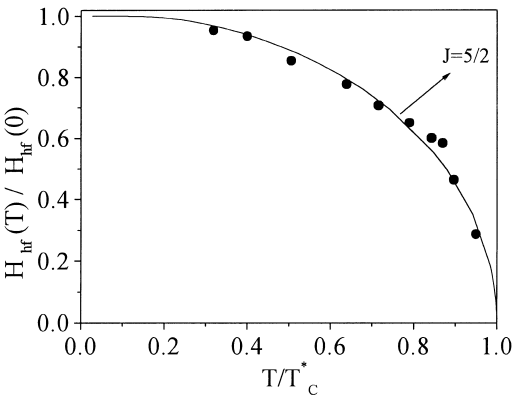

Fig. 22. Normalized hyperfine field as a function of normalized temperature of sextet B.

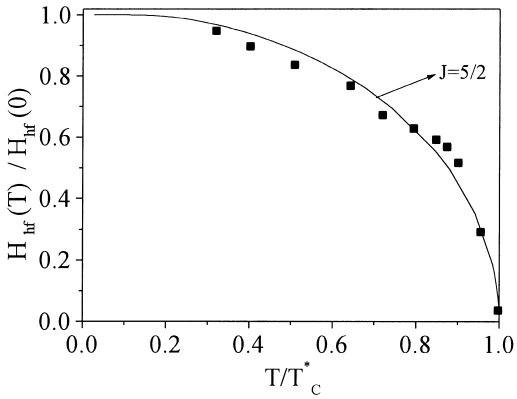

Fig. 23. Normalized hyperfine field as a function of normalized temperature of sextet C.

Table 1
Room temperature isomer shifts δ (with respect to iron), room temperature and zero kelvin hyperfine magnetic fields (H_{hf}), Curie temperature (T_C^*) and relative Zeeman percentage (%Z) of each of the subspectra obtained for the sample heat treated at 900 K. In all cases, the linewidths (Γ) were 0.35 mm/s

	δ (mm/s)	$H_{hf}(0)$ (T)	H_{hf} (300 K) (T)	T_C^* (K)	%Z
Sex A	0.07	33.0	32.1	900	37
Sex B	0.10	30.0	28.6	940	11
Sex C	0.13	25.0	23.7	935	52

The following step was to identify the crystalline phases. To assure complete crystallization of the material, a sample was heat treated in the manner described above. The pre-identification of these phases came through the room temperature Mössbauer parameters of the three obtained subspectra (labeled as Sex A, B and C), which are shown in Fig. 11, together with a study of the temperature variation of the three hyperfine fields, which were also fitted to universal Brillouin curves (Figs. 21–23). The Curie temperatures and the zero temperature field values were obtained extrapolating these curves. These results, together with the room temperature fields, the isomer shifts and the relative Zeeman percentage of each subspectra are shown in Table 1.

Despite the Curie temperature and the intensities of the hyperfine fields at room temperature and zero kelvin being lower than the corresponding quantities of crystalline bcc α-Fe [13], we identify Sex A with this phase with a small amount of Si impurities. In fact, it is known that the Curie temperature of α-Fe decreases from 1042 to 772 K as the silicon content increases from 0 to 15 wt% [15]. For the Curie temperature obtained in our experiment (900 K), an estimate of 7.9 wt% of silicon can be made.

On the other hand, the Mössbauer parameters and extrapolated zero temperature field and Curie temperature of Sex C correspond to tetragonal Fe_2B [16].

The assignment of Sex B, however, is not so clear. It could be either a Fe–Si solid solution or to the cubic Fe_3Si phase.

The observed differences could also be understood in terms of the total angular momentum obtained from the fitting process in each case ($J = \frac{3}{2}, \frac{5}{2}$, and $\frac{5}{2}$, respectively). These values indicate that, even if the amorphous material has crystallized, the crystalline fields of the different phases are lower than in the usual crystalline phases. As it will be seen in what follows during the crystallization process only nanocrystals are formed, so the local crystalline field is only due to the nearest neighbors and, consequently, the electron spin paring should be smaller than in the whole crystal ($J = \frac{1}{2}$ in α-Fe) [17].

As can be seen in the X-ray diffractograms (Fig. 17), the as-cast ribbon shows a broad peak indicating the amorphous character of the material (Fig. 17a). The gradual evolution towards the crystalline state of the sample heated during 12, 18 and 48 h is seen in the diffractograms Figs. 17b–d. It is interesting to note that the broad peak in the amorphous material is centered at $2\theta \approx 45^\circ$, the same angle where the strongest peak of the crystallized sample will appear after 48 h of heat treatment. As has been pointed out elsewhere [18], the amorphous material contains nuclei of the crystalline grains.

The final phase identification was made comparing the X-ray diffractogram of the sample heated during 48 h (Fig. 24) with the standard diffraction patterns [19]. There is a clear connection between the observed peaks and the ones corresponding to the cubic α-Fe and tetragonal Fe_2B. The peaks that could be associated with a third phase are very feeble, or they are superimposed to other peaks. So no clear identification of this phase can be made. However, considering the nominal composition of the material and the Mössbauer results, the third phase could be a solid solution of α-Fe and Si, or the cubic Fe_3Si phase. The crystal lattice parameters are shown in Table 2.

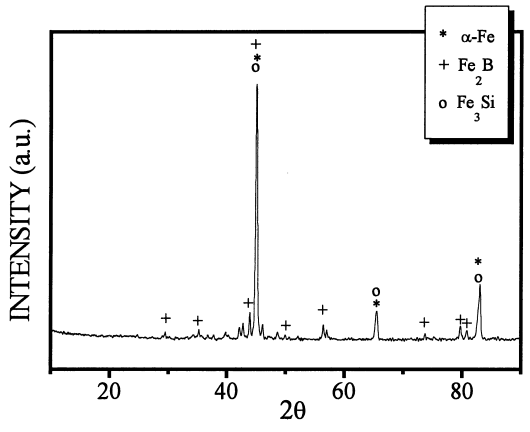

Fig. 24. X-ray diffractogram of the crystallized sample.

Table 2
Lattice parameters for the crystalline phases

	a (Å)	b (Å)	c (Å)
Fe_2B	5.0985	5.0985	4.2297
α-Fe	2.8440	2.8440	2.8440

The first TEM MG-EDP, taken at room temperature, reveals the amorphous character of the as-cast sample. However, after 3 min at 673 K, a large fraction of the material has crystallized and the second diffraction ring starts to show the typical fragmentation of a crystalline state. This early crystallization is probably due to a local heating provoked by the electron beam of the microscope (≈ 100 K). The subsequent MG shows an increase in the nanocrystal density, but not in their average size (10–20 nm). The EDP rings show a corresponding increasing fragmentation. The interplanar distances, d_{exp}, were calculated measuring the diffraction rings radius, R_{exp}, of the sample heated during 61 min. These distances were compared with PDF tables. Unfortunately, the interplanar distances concur with the three phases (Table 3), so an unambiguous identification cannot be made.

5. Conclusion

The in situ study reveals that the broad peak in the DSC curve observed around 700 K is associated with the ferromagnetic to paramagnetic state transition of the amorphous material. The magnetic field originally present in the amorphous phase has a 'normal' behavior, in the sense that it

Table 3
EDP ring radius (R_{exp}) of the sample heated during 61 min at 673 K; calculated interplanar distances (d_{expl}), PDF tables interplanar distances and Miller indices of the reflecting planes of the three identified phases

R_{exp} (cm)	d_{exp} (Å)	d(α-Fe) (Å)	(h, k, l) (α-Fe)	d(Fe_3Si) (Å)	(h, k, l) (Fe_3Si)	d(Fe_2B) (Å)	(h, k, l) (Fe_2B)
1.24	2.02	2.01	(1, 1, 0)	2.005	(1, 0, 0)	2.01	(1, 0, 0)
1.75	1.43	1.43	(2, 0, 0)	1.42	(2, 0, 0)	—	—
2.47	1.01	1.01	(2, 2, 0)	—	—	1.05	(3, 3, 2)
2.77	0.90	0.90	(3, 1, 0)	—	—	0.90	(5, 1, 2)

can be described by Weiss molecular field theory. The total angular momentum of the iron atoms turns out to be $\frac{5}{2}$ and this implies Fe^{3+} in which the electronic spins are uncoupled. Once T_c is achieved, a crystallization process begins, giving place to three crystalline magnetic phases.

On the other hand, the Curie temperatures of the nanocrystalline phases were also determined. The magnetic behavior of these phases is also described by universal Brillouin curves with $J_1 = \frac{3}{2}, J_2 = \frac{5}{2}$ and $J_3 = \frac{5}{2}$.

Finally, two of the three phases in which the system crystallizes were identified as α-Fe and Fe_2B. The third phase could be the cubic phase of Fe_3Si or a solid solution of α-Fe(Si).

Acknowledgements

The authors would like to acknowledge C. Vázquez, for the DSC measurements, and to C. Munive and J.L. Pérez Mazariego for his help in preparing the manuscript. This work was partially supported by DGAPA, México, Project IN102896.

References

[1] U. Gonser, Atomic Energy Rev. (Suppl.) 1 (1981) 203.
[2] R. Hasegawa, J. Magn. Magn. Mater. 100 (1991) 1.
[3] A. Gubanov, Fiz. Tver. Tela. 2 (1960) 502.
[4] M. Vázquez, P. Marín, H.A. Davies, A.O. Olofinjana, Appl. Phys. Lett. 64 (1994) 3184.
[5] P.W. Anderson, Survey of theories of spin glass, in: R.A. Levy, R. Hasegawa (Eds.), Amorphous Magnetism II, Plenum Press, New York, 1977, p. 1.
[6] C.L. Chien, Phys. Rev. B 18 (1978) 1003.
[7] K. Handrich, Phys. Stat. Sol. 32 (1969) K55.
[8] S. Kobe, Phys. Stat. Sol. 41 (1970) K13.
[9] M. Fähnle, J. Magn. Magn. Mat. 210 (2000) 1.
[10] K. Scröeder, Electronic, Magnetic, and Thermal Properties of Solid Materials, Marcel Dekker, New York, 1978, pp. 198–199.
[11] N.N. Greenwood, T.C. Gibb, Mössbauer Spectroscopy, Chapman & Hall, London, 1971, pp. 50–53.
[12] F. van der Woude, Phys. Stat. Sol. 17 (1966) 417.
[13] R.S. Preston, S.S. Hanna, J. Heberle, Phys. Rev. 138 (1962) 2207.
[14] G. Herzer, IEEE Trans. Mag. 21 (1989) 3327.
[15] S. Chikazumi, Physics of Ferromagnetism, Clarendon Press, Oxford, 1997, p. 601.
[16] L. Takacs, M.C. Cadeville, I. Vincze, J. Phys. F 5 (1975) 800.
[17] M. Ghafari, R. Gómez Escoto, Hyp. Interact. 110 (1997) 51.
[18] F.E. Fujita, Atomic Energy Rev. (Suppl.) 1 (1981) 173.
[19] International Centre for Diffraction Data, 1997.